Materials Science & Engineering B 226 (2017) 177–187

Contents lists available at ScienceDirect

Materials Science & Engineering B

journal homepage: www.elsevier.com/locate/mseb

Three-dimensional $CoMoO_4$ nanorods/nanographene composites on a Ni coated macroporous electrically conductive network with excellent electrochemical performance

Yue Fu[a], Xinyao Yue[a], Liang Pan[a], Shaohui Xu[a], Yiping Zhu[a,b], Dayuan Xiong[a,b], Lianwei Wang[a,b,c,*], Paul K. Chu[c]

[a] Key Laboratory of Polar Materials and Devices, Ministry of Education, and Department of Electronic Engineering, East China Normal University, 500 Dongchuan Road, Shanghai 200241, PR China
[b] Shanghai Key Laboratory of Multidimensional Information Processing, East China Normal University, 500 Dongchuan Road, Shanghai 200241, PR China
[c] Department of Physics and Department of Materials Science and Engineering, City University of Hong Kong, Tat Chee Avenue, Kowloon, Hong Kong, China

ARTICLE INFO

Keywords:
Macroporous electrically conductive network (MECN)
Nanographene
$CoMoO_4$ nanorods
Composite electrode
Hybrid device

ABSTRACT

Nanostructured three-dimensional (3D) $CoMoO_4$ nanorods/nanographene composites were produced on a macroporous electrically conductive network (MECN). The nanographene with more defects serving as the active center enhances the conductivity and faradic charge transfer of the composite, and more, the porous 3D structure of the MECN increases the specific area, improves the mass loading of active materials, and enhances transport behaviors of ion and electron, leading to large specific capacity and excellent rate capability. The $CoMoO_4$/nanographene/MECN electrode has a capacity of 85.5 mA h/g (855 μA h cm^{-2}) at a discharge current density of 1 A g^{-1} (10 mA cm^{-2}) and capacity loss of 13.6% after 5000 cycles. The hybrid device composed of $CoMoO_4$/nanographene/MECN ll AC/Ni-foam exhibits excellent capacities of 112.4 μW h cm^{-2} and 5.62 mW h cm^{-3} at power densities of 675.5 μW cm^{-2} and 33.78 mW cm^{-3}, respectively, in addition to 74.4% capacity retention after 5000 cycles.

1. Introduction

Much attentions are being paid to advanced energy storage systems [1–3] and supercapacitors including electrochemical double layer capacitors (EDLCs) and pseudocapacitors (PCs) are potential candidates due to the high power density, long cycling life, fast charging/discharging rate, and high reliability [4–8]. Different from carbon-based electrochemical double layer capacitors (EDLCs), pseudocapacitors (PCs) have larger energy densities because the energy is stored based on the reversible faradic reactions inside the electrode instead of charge accumulation at the electrolyte/electrode interface in the EDLCs [9,10]. Various single-component transition metal oxides such as MnO_2 [11,12], Co_3O_4, [13,14] RuO_2 [15], and NiO [16,17] have been developed as the faradic electrode. In addition, MnO_2 has several merits as pseudocapacitive materials, for instance, the high specific capacitance, low cost, and nontoxicity, however the poor electrical conductivity has hampered wider adoption [18,19]. In comparison, RuO_2 also has large specific capacitances but the high cost and toxicity are drawbacks [20] (see Table 1).

In addition to the aforementioned single-component transition metal oxides, binary metal oxides such as $MnMoO_4$ [21], $ZnCo_2O_4$ [22], $NiMoO_4$ [23], and $CoMoO_4$ [24] have good electrochemical properties because of high electrical conductivity in the oxidation states. In particular, $CoMoO_4$ has attracted much attention because it is non-toxic and economical and delivers good electrochemical performance due to the combination of high specific capacitance of Co_2O_3 and reversible small ion storage and rich polymorphism of MoO_3 [25,26]. Since nanostructures can increase the contact area more between the electrode and electrolyte and facilitate electrolyte transportation, nanostructured $CoMoO_4$ such as $CoMoO_4$ nanoplate arrays [20], hierarchical $CoMoO_4$ nanoflakes [27], $CoMoO_4$ nanorods [28], and $CoMoO_4$ nanospheres [29] have been proposed and synthesized. The $CoMoO_4$ nanoflakes fabricated by Li et al. exhibited a large specific capacity of 32.40 mA h g^{-1} at a current density of 1 A g^{-1} and excellent rate capability [27] and the $CoMoO_4$ nanorods synthesized by Liu et al. showed a high specific capacitance of 286 F g^{-1} at a current density of 5 mA cm^{-2} [28]. Furthermore, fabricating nanocomposites with highly conductive materials such as carbon spheres, carbon nanotubes (CNTs), and

* Corresponding author at: Key Laboratory of Polar Materials and Devices, Ministry of Education, and Department of Electronic Engineering, East China Normal University, 500 Dongchuan Road, Shanghai 200241, PR China.
E-mail address: lwwang@ee.ecnu.edu.cn (L. Wang).

http://dx.doi.org/10.1016/j.mseb.2017.09.019
Received 5 July 2017; Received in revised form 16 September 2017; Accepted 26 September 2017

Table 1
The common abbreviations in this paper.

Si-MCPs	silicon microchannel plates
MECN	macroporous electrically conductive network
EDLCs	electrochemical double layer capacitors
PCs	pseudocapacitors
AC/Ni-foam	active carbon/Ni-foam
PE	poly-ethylene
CV	cyclic voltammetry

graphene can improve the electrical conductivity of the electrode. The $CoMoO_4$/carbon nanotube composites reported by Xu et al. had a high specific capacitance of 170 F g^{-1} at a discharge current density of 0.1 A g^{-1} [30] and Xia et al. reported that the CoMoO4/graphene composites had low electrochemical resistance and large specific capacitance of about 394.5 F g^{-1} according to CV curves obtained at 1 mV s^{-1} [31].

In this work, multilayered nanographene is prepared on the macroporous and electrically conductive network (MECN) by hydrothermal carburization [32]. The MECN prepared by the micro-electro-mechanical system (MEMS) technology and electro-less deposition of nickel [33–36] has an ordered porous and stable architecture which supports the nanographene while avoiding aggregation to turn into graphite. The three-dimensional macroporous structure of MECN also facilitates access of electrons and electrolyte ions to the active surface and improves the electrochemical response on the electrode. Compared to MECN, nanographene/MECN has a larger specific area, active surface, and better electrical conductivity due to defects in the nanographene. The ordered $CoMoO_4$ nanorods are prepared on the nanographene/MECN electrode hydrothermally for different time durations of 0.5, 1.5, 2.5, and 3 h. The $CoMoO_4$ nanorods are formed on the surface and the micro-channels in nanographene/MECN provide a large surface area for the active materials. The nanostructured $CoMoO_4$/nanographene/MECN composites electrodes are studied systematically and the electrochemical performance as a faradic electrode is determined.

2. Experimental details

2.1. Chemicals and materials

All the chemical reagents were of AnalaR grade and used as received without further purification. Nickel chloride ($NiCl_2{\cdot}6H_2O$), ammonium chloride (NH_4Cl), ethanol, sodium hypophosphite ($NaH_2P_2{\cdot}H_2O$), sodium acetate ($C_3H_3NaO_2$), triethylene glycol ($C_6H_{14}O_4$), cobalt chloride hexahydrate {$CoCl_2{\cdot}6H_2O$}, and ammonium molybdate tetrahydrate [$(NH_4)_6Mo_7O_{24}{\cdot}4H_2O$] were purchased from Sinopharm Chemical Reagent Co. Ltd. The aqueous solutions were prepared with de-ionized water.

2.2. Fabrication of the macroporous electrically conductive network (MECN)

The silicon microchannel plates (Si-MCPs) were fabricated by electrochemical etching of p-type silicon [33,34] and electroless deposition of Ni was performed in a plating bath by liquid flowing deposition [35,36]. The Si-MCPs were dipped in a solution composed of HF: C_2H_5OH:H_2O (100:125:10, V/V) for 2 min to remove the native oxide and immersed in a plating bath for 18 min at 90 °C. The plating solution was prepared by dissolving 3 g of $NiCl_2{\cdot}6H_2O$, 5 g of NH_4Cl, and 1 g of $NaH_2PO_2{\cdot}H_2O$ in 100 ml of deionized water and 30 ml of NH_4OH were added to maintain the pH of the platting solution between 9 and 11.

2.3. Fabrication of nanographene/MECN

5 ml of 1 M sodium oxalate ($C_3H_3NaO_2$) were dissolved in 100 ml of triethylene glycol ($C_6H_{14}O_4$) and stirred for 40 min with a magnetic stirrer. The Ni/Si-MCPs (MECN) were introduced into the solution and sonicated for 5 min to let the solution fill the channels (5 × 5 × 200 μm, length × width × height) in the MECNs. The MECNs and solution were then put in a Teflon-sealed stainless steel autoclave and placed in a vacuum oven heated to 260 °C. The temperature was maintained for 6 h to produce the carbon-nickel alloyed Ni_3C/MECN. After the autoclave was cooled naturally to room temperature, the Ni_3C/MECN samples were washed with de-ionized water for 20 min and dried at 80 °C in vacuum oven for 6 h. Afterwards, the

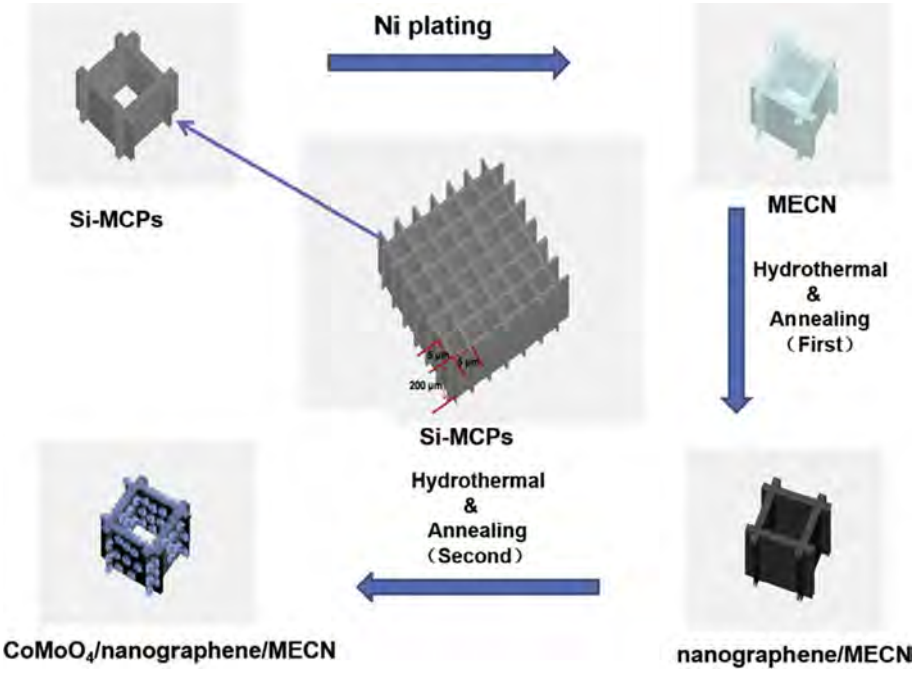

Fig. 1. Illustration of procedures to fabricate the $CoMoO_4$/nanographene/MECN electrode.

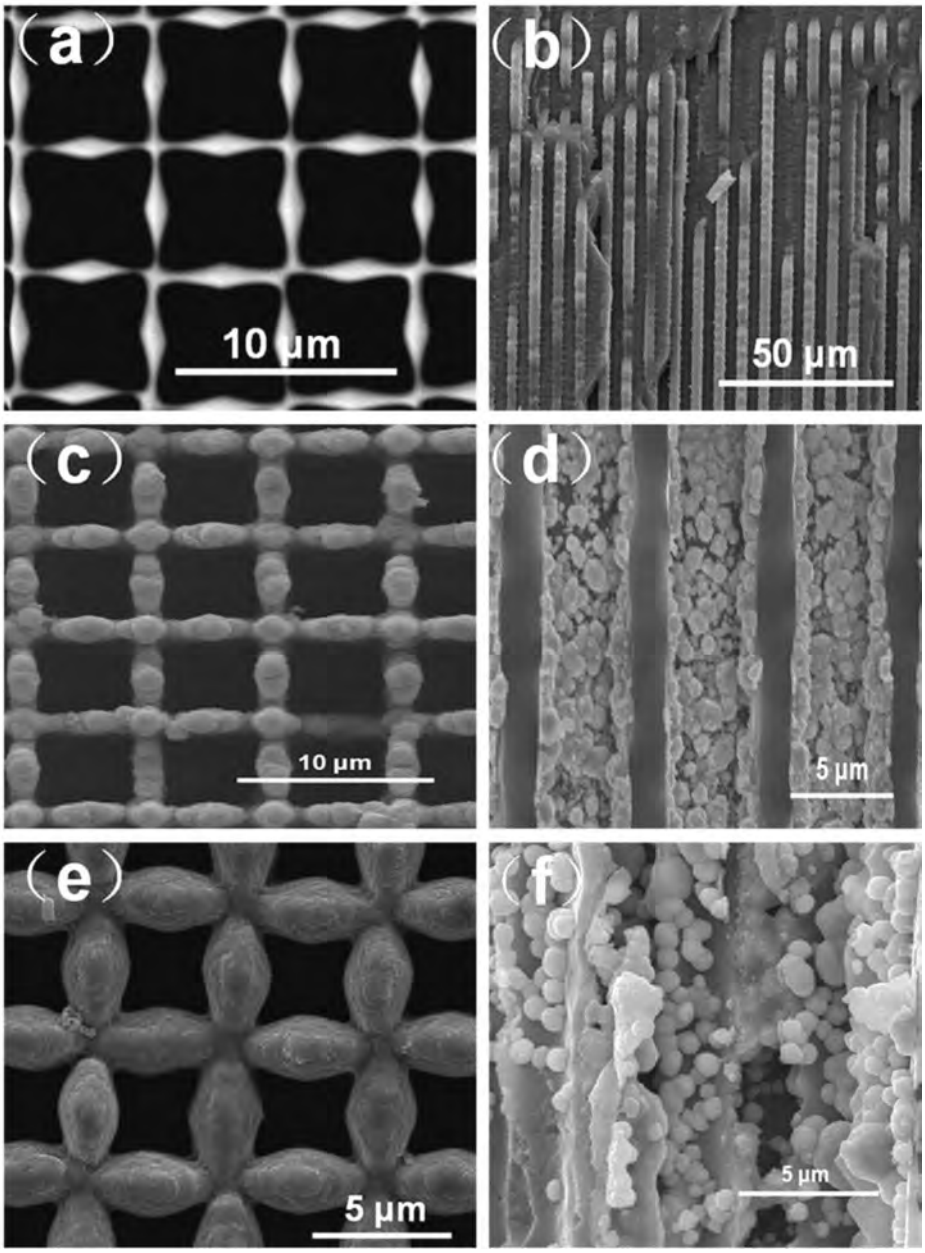

Fig. 2. FE-SEM images: (a) Top surface of the Si-MCPs, (b) Cross-sectional morphology of the Si-MCPs, (c) Top surface of MECN, (d) Cross-sectional morphology of the MECN, (e) Top surface of nanographene/MECN, and (f) Cross-sectional morphology of the nanographene/MECN.

samples were placed in a tube furnace and annealed at 650 °C for 1 h under argon atmosphere to obtain the nanographene/MECN. The Ni_3C phase is unstable at temperatures between 325 °C and 480 °C and it will completely decomposes into a mixture of nickel phases and graphite phases after annealing at 650 °C due to the carbon segregation. More details about the process can be found in [37]. The decomposition reaction for Ni_3C in argon atmosphere can be described as following:

$$Ni_3C(s) = 3Ni(s) + C(s) \quad (1)$$

2.4. Fabrication of nanostructured $CoMoO_4$/nanographene/MECN and $CoMoO_4$/ MECN

The $CoMoO_4$ nanorods were prepared directly on nanographene/MECN or MECN hydrothermally. The solution was produced by mixing 0.6 mmol $CoCl_2{\cdot}6H_2O$ and 0.6 mmol $(NH_4)_6Mo_7O_{24}{\cdot}4H_2O$ in 150 ml of deionized water under magnetic stirring. The solution and nanographene/MECN (or MECN) were transferred to a Teflon-sealed stainless steel autoclave and kept at 180 °C for 0.5 h, 1.5 h, 2.5 h, or 3 h [samples designated as $CoMoO_4$/nanographene/MECN (0.5 h, 1.5 h, 2.5 h, 3 h) or $CoMoO_4$/ MECN (0.5 h, 1.5 h, 2.5 h, 3 h)]. Afterwards, the samples were removed from the autoclave, washed with deionized water and ethanol few times, and dried in an oven at 80 °C for 6 h. The nanographene/MECN or MECN with the as-grown hydrate precursors was annealed at 300 °C for 2 h under argon to obtain the nanostructured $CoMoO_4$/nanographene/MECN or $CoMoO_4$/ MECN. The reaction is described in Eq. (2) [30]:

$$(NH_4)6Mo_7O_24{\cdot}4H_2\ O + 7CoCl_2{\cdot}6H_2\ O \rightarrow 7CoMoO_4 + 6NH_3 + 14HCl + 42H_2O \quad (2)$$

2.5. Assembly of the hybrid device

In the hybrid device, the $CoMoO_4$/nanographene/MECN (2.5 h) was the anode, active carbon/Ni-foam (marked as AC/Ni-foam) was the cathode, and 2 M KOH was the electrolyte. The AC/Ni-foam electrode was fabricated by a coating method [38]. The active carbon (80 wt%), polytetrafluoroethylene suspension (10 wt%), and acetylene black

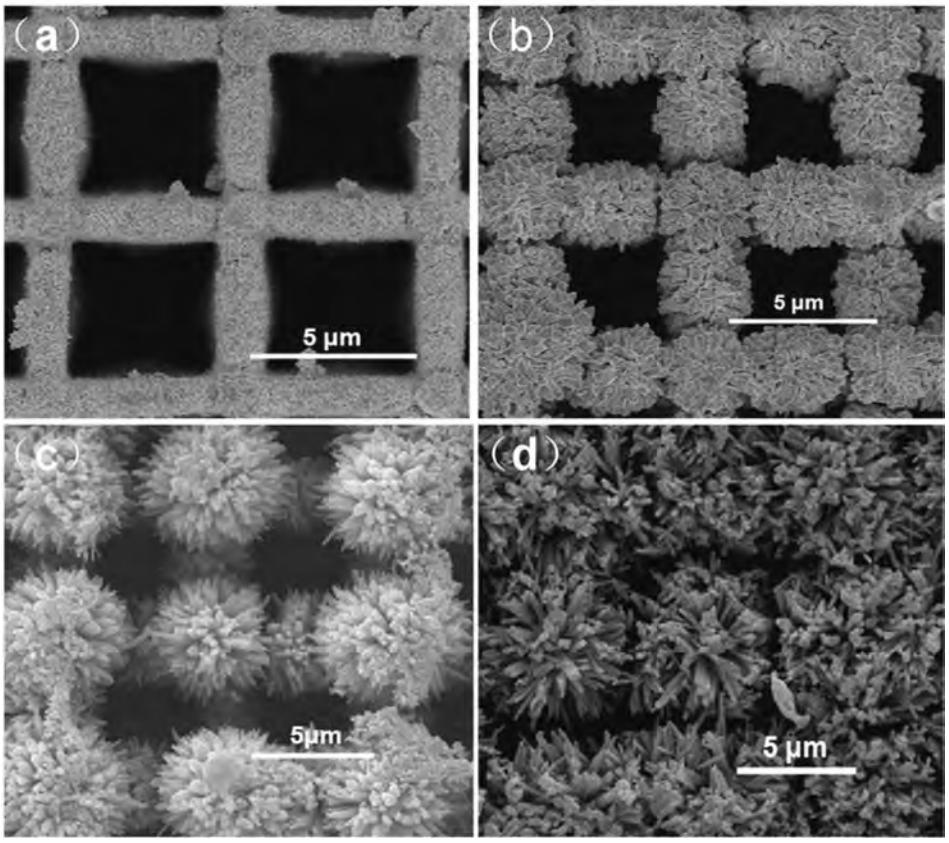

Fig. 3. Top surface FE-SEM images of the $CoMoO_4$/nanographene/MECN prepared for different hydrothermal time: (a) 0.5 h, (b) 1.5 h, (c) 2.5 h, and (d) 3 h.

(10 wt%) were dispersed in isopropanol and sonicated for 30 min to get a homogeneous slurry. The slurry was uniformly coated onto the nickel foam substrate and dried in a vacuum oven overnight at 60 °C to produce the active carbon/Ni-foam electrode. The anode and cathode were separated by a poly-ethylene (PE) membrane and assembled in a RS2032 battery case.

2.6. Materials characterization

The microstructure and morphology were characterized by field-emission scanning electron microscopy (FE-SEM, Hitachi S-4800, Japan) and high-resolution transmission electron microscopy (HR-TEM, JEM-2010F). The crystal structure and elementary composition were measured by X-ray diffraction (XRD, Rigaku, RINT2000, Japan), Raman scattering (T6400 Jobin Yvon triple monochromator, Tokyo, Japan, using a 532 nm argon ion laser), X-ray photoelectron spectroscopy (XPS; Kratos AXIS Ultra DLD) and energy-dispersive X-ray spectrometry (EDS) (Fig. 1).

2.7. Electrochemical measurements

The electrochemical characteristics of the electrodes were determined on an electrochemical workstation (Shanghai Chenhua, CHI660D) in 2 M KOH. The saturated calomel electrode and platinum foil served as the reference electrode and counter electrode, respectively. The cyclic voltammetry (CV) scans were acquired from 0 to 0.6 V at different scanning rates and galvanostatic charging-discharging was conducted in the potential range between 0 and 0.45 V. The CV scans were obtained from the hybrid device from 0 to 1.6 V at different scanning rates and the galvanostatic charging-discharging cycling tests were conducted in the potential range between 0 and 0.9 V.

3. Results and discussion

3.1. Discussion of the fabrication process of $CoMoO_4$/nanographene/MECN electrode

As shown in Fig. 2(a) and (b), the micro-channels of Si-MCPs have a depth of about 200 μm and size of 5 × 5 μm giving an aspect ratio about 40 and the surface area gain can be larger than 100. Fig. 2(c) and (d) depict the FE-SEM images of the MECN. After electroless Ni plating, a thin nickel particulate layer about 0.5 μm thick uniformly covers the sidewall and surface of the Si-MCPs to provide good electrical conductivity. The porous nickel particles increase the specific surface of the MECN [Fig. 2(e)] and the nanographene is uniformly coated on the nickel particles in the channels of the MECN. The nanographene/MECN retains the original 3D morphology of the MECN after annealing at 650 °C.

Fig. 3 shows the growth of the $CoMoO_4$ nanorods. The nanostructured $CoMoO_4$ resemble small nanodots (Fig. 3a) and nanoflakes (Fig. 3b) on the surface of the supporting materials in the early nucleation stage. As shown in Fig. 3(b), the nanostructured $CoMoO_4$ preferentially grows on the middle of the wall and crossing points of the nanographene/MECN because there have a larger area (Fig. 2 e) for the growth of heteromorphic $CoMoO_4$. As time elapses, the nanostructured $CoMoO_4$ layer becomes thicker and the $CoMoO_4$ nano-flakes transform into $CoMoO_4$ nanorods (Fig. 3c). As shown in the Fig. 3(c), the crossing points of MECN form the nucleation centers for the growth of the $CoMoO_4$ nanorods. As the hydrothermal time is increased further (Fig. 3d), the cubic holes of the substrate are blocked by the $CoMoO_4$ nanorods which are unfavorable to the transport of electrolyte ions.

3.2. Characterization of the $CoMoO_4$/nanographene/MECN composites

Fig. 4 (a)–(c) show the top-view morphology of the $CoMoO_4$ nanorods. The diameter of a single nanorod is about 100 nm. The

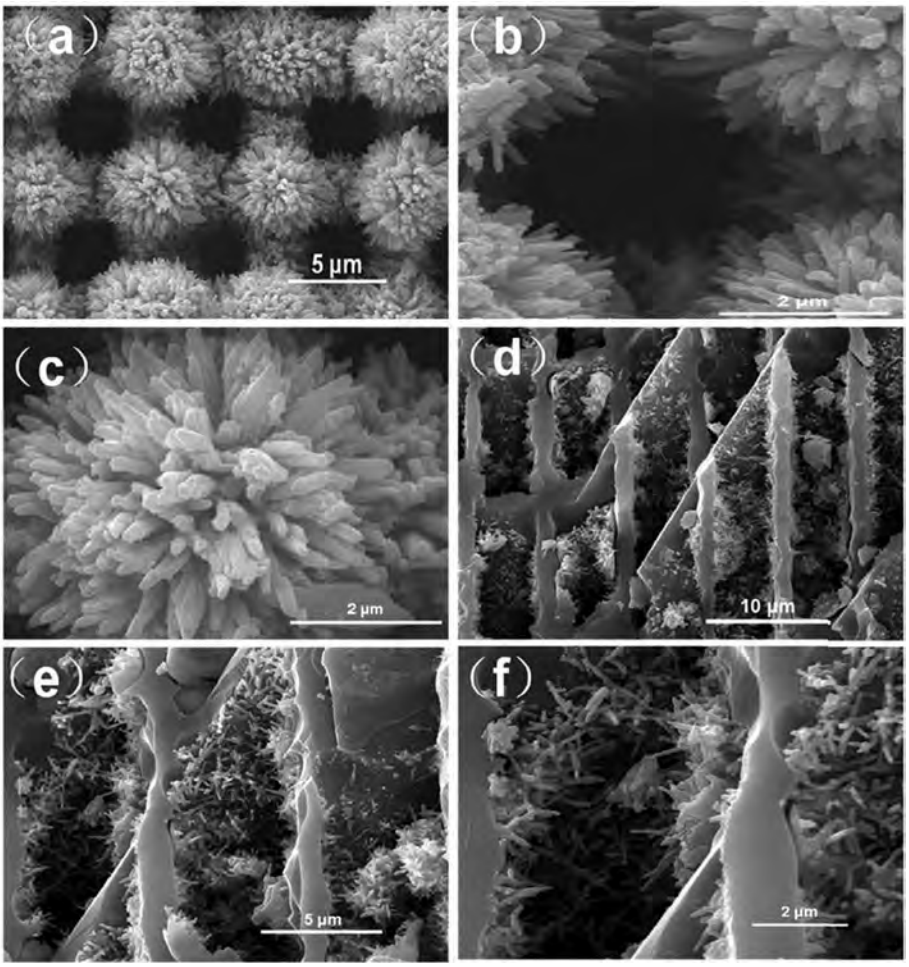

Fig. 4. FE-SEM images: (a)–(c) Top surface of the $CoMoO_4$/nanographene/MECN (2.5 h) at different magnifications, (d)–(f) Cross-sectional morphology of the $CoMoO_4$/nanographene/MECN (2.5 h) at different magnifications.

nanorods can further improve the specific surface area which is important to the active materials capacity. As shown in Fig. 4(d)–(f), the $CoMoO_4$ nanorods are also formed in the microchannels of the nanographene/MECN, thus improving the performance of the electrode by providing more electroactive sites for the reactions and increasing the total contact area between the active materials and electrolyte.

The chemical composition and phase structure of the samples are determined by EDS, Raman scattering, and X-ray diffraction (XRD). Fig. 5 (a) shows that the nanographene/MECN contains carbon, nickel and silicon and the atomic ratio of carbon to the other elements are 19.66% and 46.09% respectively, indicating that multilayered nanographene is synthesized on the MECN by hydrothermal carburization. As shown in Fig. 5 (b), the $CoMoO_4$/nanographene/MECN contains carbon, oxygen, nickel, silicon, molybdenum, and cobalt. Fig. 5 (c) shows the Raman spectrum of the $CoMoO_4$/nanographene/MECN and peaks at 335, 373, 821, 887, 940, 1350, and 1580 cm^{-1}. According to previous reports [21,38,39], the Raman bands at 880 and 940 cm^{-1} and broad band at 350 cm^{-1} correspond to Mo–O–Co stretching vibrations in cobalt molybdate. The bands at 812 and 332 cm^{-1} are attributed to MoO_4 vibrations whereas those at 1350 cm^{-1} (D band) and 1580 cm^{-1} (G band) are characteristic peaks of nanographene indicating the nanographene have not aggregated into graphite after the preparation of $CoMoO_4$ nanorods [40]. The strong D band demonstrates that the nanographene coated on MECN has many defects which increase the electrochemically active surface for absorption/desorption of OH^- and improves the electrochemical performance of the $CoMoO_4$/nanographene/MECN electrode. Fig. 5 (d) depicts the phase changes in MECN, Ni_3C/MECN, nanographene/MECN, and $CoMoO_4$/nanographene/MECN. The MECN exhibits three peaks from the cubic phase Ni metal [JCPDS card No. 70-1849, marked with a hollow diamond, with the peak (1 1 1) at $2\theta = 44.7^\circ$, peak (2 0 0) at $2\theta = 52.1^\circ$, and peak (2 2 0) at $2\theta = 76.6^\circ$] and the rest stems from the Si substrate [marked with a solid diamond, with peak (4 0 0) at $2\theta = 69.3^\circ$]. After the first hydrothermal process, the peak of nickel carbide [JCPDS card No. 77-0194, marked with a circle, with peak (2 1 2) at $2\theta = 39.1^\circ$, peak (4 1 1) at $2\theta = 41.6^\circ$, peak (3 1 2) at $2\theta = 44.6^\circ$, peak (6 1 1) at $2\theta = 58.4^\circ$, peak (4 3 3) at $2\theta = 71.2^\circ$, peak (3 1 4) at $2\theta = 78.1^\circ$] shows that carbon permeates into the Ni nanoparticles. After annealing at 650 °C for 1 h in argon, the nickel carbide peaks disappear and a broad peak at $2\theta = 24^\circ$of graphite (0 0 2) appears from the nanographene/MECN. The peak of $CoMoO_4$ (JCPDS card No. 00-021-0868) in the XRD patterns of the $CoMoO_4$/nanographene/MECN electrode indicates that heteromorphic $CoMoO_4$ is synthesized. Fig. 5 (e) shows the typical TEM image of $CoMoO_4$ nanorods and as shown in the HR-TEM image in Fig. 5 (f), the interplanar spacing of 0.33 nm corresponds to the (0 0 2) plane of the $CoMoO_4$, which is consistent with the crystal structure of $CoMoO_4$ in the XRD pattern in Fig. 5(d).

In order to further analyze the existence of covalent bonds in the samples, X-ray photoelectron spectroscopy spectra were acquired in Fig. 6. As shown in Fig. 6 (a), the sample contains Ni, C, Mo, Co and O element. The C 1s core-level spectrum of $CoMoO_4$/nanographene/MECN (Fig. 6 b) show four peaks with binding energies at about 284.5, 285.4, 286.7, and 288.6 eV, attributable to the sp^2 hybridized carbon, sp^3 hybridized carbon, C-O, and C-OO species, respectively. Fig. 6 (c) depicts the XPS spectrum of Mo 3d with the binding energies at 232.1 and 235.2 eV which corresponding to Mo $3d_{5/2}$ and Mo $3d_{3/2}$ respectively. The binding energy and splitting width (ΔMo 3d = 3.1 eV) are in good agreement with Mo^{6+} [31]. The Co 2p core-level spectrum (Fig. 6

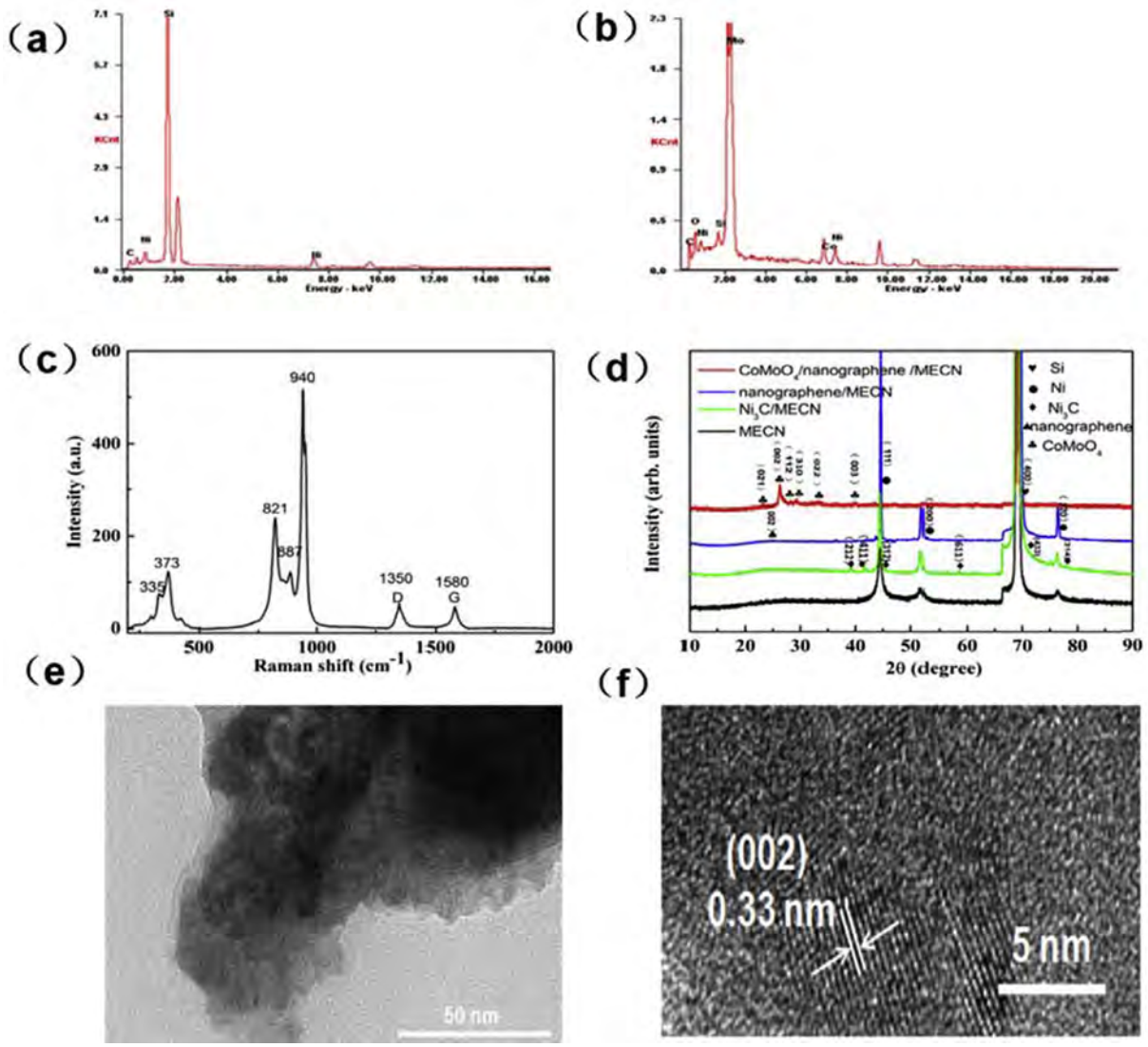

Fig. 5. EDS spectra of (a) Nanographene/MECN and (b) $CoMoO_4$/nanographene/MECN; (c) Raman scattering spectrum of $CoMoO_4$/nanographene/MECN; (d) XRD patterns of MECN, Ni_3C/MECN, nanographene/MECN, and $CoMoO_4$/nanographene/MECN; (e) Low-magnification TEM image of the $CoMoO_4$ nanorods; (e) High-resolution TEM image of the $CoMoO_4$ nanorods.

d) displays two peaks at 782.6 and 798.2 eV, attributing to the Co $2p_{3/2}$ and Co $2p_{1/2}$, respectively, which belongs to Co^{2+} [31].

3.3. Electrochemical characterization

To evaluate the electrochemical performance of the different electrodes, cyclic voltammetry (CV) and chronopotentiometry are conducted. Fig. 7 (a),(b) disclose that the $CoMoO_4$/nanographene/MECN (2.5 h) has the largest capacity because of the large enclosed area in the CV curve (10 mV s^{-1}) and longest discharging time. Compared to $CoMoO_4$/nanographene/MECN (0.5 h and 1.5 h), $CoMoO_4$/nanographene/MECN (2.5 h) has more abundant $CoMoO_4$ nanorods to provide a larger active area. With regard to $CoMoO_4$/nanographene/MECN (3 h), the abundant nanorods of $CoMoO_4$ block the microchannels in the backbone materials consequently reducing the contact area between the electrolyte and active substance. As shown in the Fig. 7 (c), the MECN electrode contributes negligibly to the capacity and the enclosed area in the CV curve of the $CoMoO_4$/nanographene/MECN electrode is large than that of the $CoMoO_4$/MECN and nanographene/MECN electrodes, indicating the highest capacity. Fig. 7 (d) reveals that the $CoMoO_4$/nanographene/MECN electrode has the longest discharging time demonstrating that it has the highest specific capacity than the other electrodes.

Fig. 8 (a) shows the CV curves of the $CoMoO_4$/nanographene/MECN (2.5 h) electrode at different scanning rates in 2 M KOH. The peak current increases with scanning rates. The peak shape is similar exhibiting apparent oxidation and reduction peaks. Nevertheless, the peak potential shifts to the cathode or anodic direction, respectively, because of more substantial polarization at larger scanning rates. The Faradic reactions correspond to the redox peaks are shown in the following [41]:

$$3[Co(OH)_3]^- \Leftrightarrow Co_3O_4 + 4H_2O + OH^- + 2e^- \quad (3)$$

$$Co_3O_4 + H_2O + OH^- \Leftrightarrow 3CoOOH + H_2O + e^- \quad (4)$$

$$CoOOH + OH^- \Leftrightarrow CoO_2 + H_2O + e^- \quad (5)$$

The reactions suggest that the electrochemical capacitance of the $CoMoO_4$/nanographene/MECN electrode is mainly attributed to the quasi reversible electron transfer process that involves the Co^{2+}/Co^{3+} redox couple and mediated by OH^- in the alkaline electrolyte. Fig. 8 (b) depicts the galvanostatic charging–discharging curves of the $CoMoO_4$/nanographene/MECN electrode at different current densities (10, 16, 20, 24, 34 mA cm^{-2}) at voltages between 0 V and 4.5 V. According to the galvanostatic charging–discharging curves, the specific

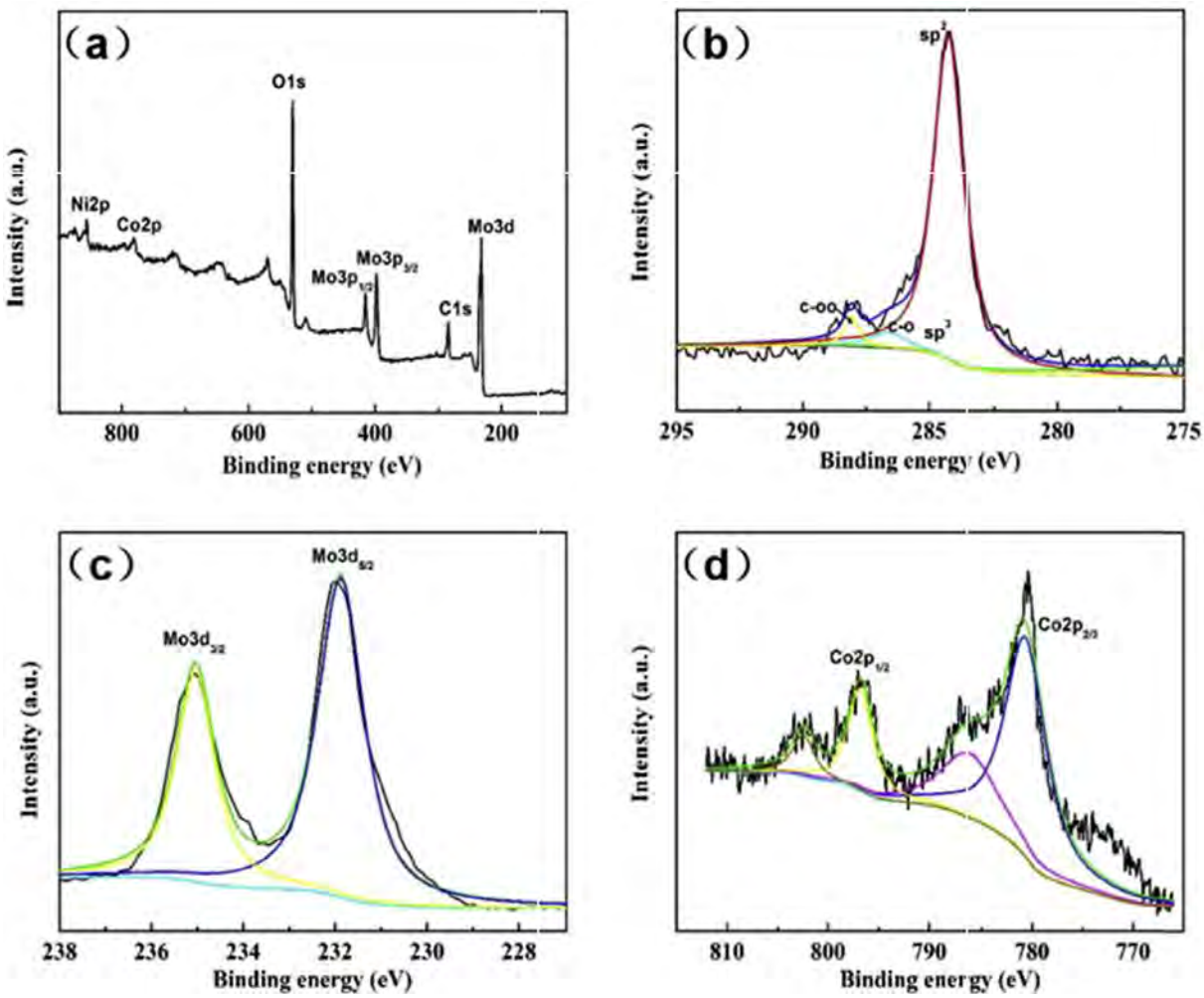

Fig. 6. XPS spectra of the $CoMoO_4$/nanographene/MECN: (a) survey spectrum, (b) C 1s core-level spectrum, (c) Mo 3d core-level spectrum and (d) Co 2p core-level spectrum.

capacities of the $CoMoO_4$/Graphene/MECN electrode are 85.5, 75.42, 70, 63.6, and 55.68 mA h g^{-1} (855, 754.2, 700, 636, and 556.8 μA h cm^{-2}) at 1.0, 1.6, 2.0, 2.4, and 3.4 A g^{-1} (10, 16, 20, 24, and 34 mA cm^{-2}) respectively. The specific capacities (85.5 mA h g and 855 μA h cm^{-2}) at a discharge current density of 1 A g^{-1} (10 mA cm^{-2}) are larger than that of the pure nano-$CoMoO_4$ (20.68 mA h g^{-1} at a discharge current of 1 A g^{-1}) described by N. Padmanathan et al. [42], hierarchical 3D $CoMoO_4$/MECN electrode (32.40 mA h at a discharge current of 1 A g^{-1}) reported by M. Li et al. [27], $CoMoO_4$/MWCNT electrode (21.33 mA h/g at a discharge current density of 1 A g^{-1}) by Xu et al. [30], and even hierarchical $CoMoO_4$@$NiMoO_4$ core–shell nanosheet arrays (458.3 μA h cm^{-2} at a discharge current of 10 mA cm^{-2}) reported by Zhang et al. [43].

As shown in Fig. 8 (c), the specific capacity of the $CoMoO_4$/nanographene/MECN electrode is larger than that of other electrodes at the same discharging current density. The specific capacity decreases with discharging current density because the charge diffusion rate of adsorption/desorption cannot catch up with the rapid increment in the charging-discharging current density. However, the specific capacity is still retained at 63.27% of its initial capacity when the charging-discharging current densities are increased from 10 to 44 mA cm^{-2}, indicating that the CoMoO4/nanographene/MECN electrode has fast charge-discharge rates and excellent rate capability.

Long-time cycle tests are carried out to determine the stability of the nanographene/MECN, $CoMoO_4$/MECN, and $CoMoO_4$/nanographene/MECN electrodes at a current density of 20 mA cm^{-2} as shown in Fig. 8 (d). The $CoMoO_4$/nanographene/MECN electrode exhibits excellent cycling stability and the capacity retention (86.4%) is better than that of the $CoMoO_4$/MECN electrode (80.5%) after 5,000 cycles due to the superior electrical conductivity of nanographene and good adhesion between the active materials and substrate.

Fig. 8 (e) shows the Nyquist plots and equivalent circuits of the electrodes. The ohmic resistance of the electrolyte and internal resistance are simulated as resistor R1 and the capacitance C1 models the double layer capacitance at the electrolyte/electrode interface. The charge transfer resistance is modeled by resistor R2 which is in series with the pseudocapacitance CPE1 [44]. As shown in the inset in Fig. 7(d), both the internal resistance and charge transfer resistance of the $CoMoO_4$/nanographene/MECN electrode (1.287 Ω and 0.0269 Ω) are smaller than those of the $CoMoO_4$/MECN electrode (3.195 Ω and 0.0530 Ω), demonstrating that the $CoMoO_4$/nanographene/MECN electrode has excellent electrical conductivity and rapid charge transfer rate. Fig. 8 (f) shows the Nyquist plots of the $CoMoO_4$/nanographene/MECN (2.5 h) electrode before and after 5000 cycles. The internal resistance R1 before and after 5000 cycles of the $CoMoO_4$/nanographene/MECN electrode is 1.287 Ω and 1.378 Ω, respectively, indicating a highly conductive electrode. After 5000 cycles, the $CoMoO_4$/nanographene/MECN electrode shows a small faradic charge transfer resistance (R2 of 0.261 Ω) demonstrating that the $CoMoO_4$/nanographene/MECN electrode has good cycling stability. In addition, the slope of the impedance plots is greater than the 45° straight line at low frequencies after 5000 cycles suggesting that the $CoMoO_4$/

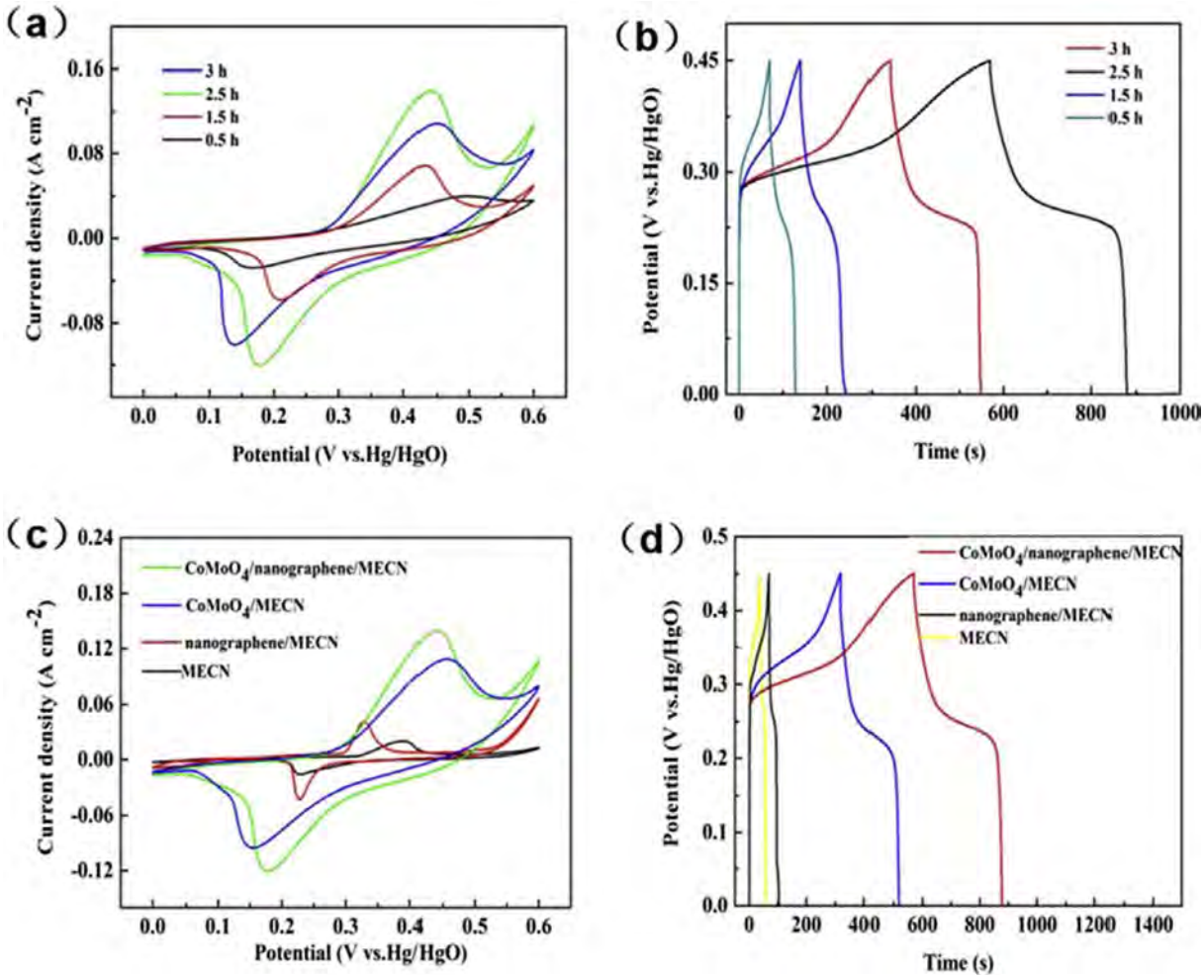

Fig. 7. (a) CV curves of the $CoMoO_4$/nanographene/MECN electrodes for different hydrothermal time; (b) Galvanostatic charging–discharging curves of the $CoMoO_4$/nanographene/MECN electrode for different hydrothermal time at a current density of 10 mA cm^{-2}; (c) CV curves of the MECN, nanographene/MECN, $CoMoO_4$/MECN (2.5 h), and $CoMoO_4$/nanographene/MECN (2.5 h) electrodes at a scanning rate of 10 mV s^{-1} in 2 M KOH; (d) Galvanostatic charging–discharging curves of the MECN, nanographene/MECN, $CoMoO_4$/MECN (2.5 h), and $CoMoO_4$/nanographene/MECN (2.5 h) electrodes at a current density of 10 mA cm^{-2}.

nanographene/MECN electrode has good capacitive behavior due to rapid ion diffusion.

For further testing, an asymmetrical hybrid device is fabricated. As shown in Fig. 9 (a), the oxidation and reduction peaks can be observed and the peak current becomes larger with scanning rates. The CV curves do not show obvious distortion at a scanning rate of 120 mV s^{-1} indicating fast charging-discharge of the hybrid device [45]. Fig. 9 (b) shows the galvanostatic charging–discharging curves of the hybrid device between 0 V and 0.9 V at different current densities. Compared to the $CoMoO_4$/nanographene/MECN electrode (0.45 V), the potential window of the hybrid device increases to 0.9 V which is beneficial to the energy density of the hybrid device. The energy densities are calculated to be 112.4 μW h cm^{-2} and 5.62 mW h cm^{-3} at power densities of 675.5 μW cm^{-2} and 33.78 mW cm^{-3}, respectively. Fig. 9 (c) presents the cycling stability of the hybrid device at a current density of 10 mA cm^{-2}. It has excellent cycling stability showing 14.6% deterioration after 3000 cycles and capacitance retention of 74.4% after 5000 cycles.

Fig. 9 (d) shows the Nyquist plots of the hybrid device before and after 5000 cycles in the long-term performance test. The ohmic resistance of the electrolyte and internal resistance are simulated as resistor R1. The constant phase-angle element CPE1 and resistor R2 are parallel to each other to simulate the solid electrolyte interface (SEI) layer. The charge transfer behavior is modeled by the capacitor C1 and resistor R3 connected parallel to each other. The Warburg impedance W1 is employed to model diffusion of OH^-. As shown on the table in Fig. 8(d), the internal resistance R1 (5.597 Ω) increases to 8.635 Ω after 7000 cycles due to damage of nanographene and Ni layer with decreasing electrical conductivity of the electrode. In addition, resistance R2 related to the SEI layer increases from 2.668 Ω to 122.2 Ω after 5000 cycles because the porous structure of the electrode is damaged during the long-term test. Resistance R3 associated with the charge transfer behavior increases to 0.78091 Ω after 5000 cycles perhaps due to damage of the $CoMoO_4$/nanographene composite active materials.

4. Conclusion

The nanostructured $CoMoO_4$/nanographene/MECN composite electrode is fabricated by a two-step hydrothermal process. The multilayered nanographene under the $CoMoO_4$ nanorods facilitates faradic charge transfer and enhances the electrochemical performance of the electrodes. The nanostructured 3D $CoMoO_4$/nanographene produced on a macroporous electrically conductive network has a large specific surface and excellent electrical conductivity, resulting in a large specific capacity of 85.5 mA h/g (855 μA h cm^{-2}) at a discharge current density of 1 A g^{-1} (10 mA cm^{-2}) and excellent capacity retention of 86.4% after 5000 cycles. The $CoMoO_4$/nanographene/MECN ll AC/Ni-foam hybrid device delivers excellent capacity performance, for example,

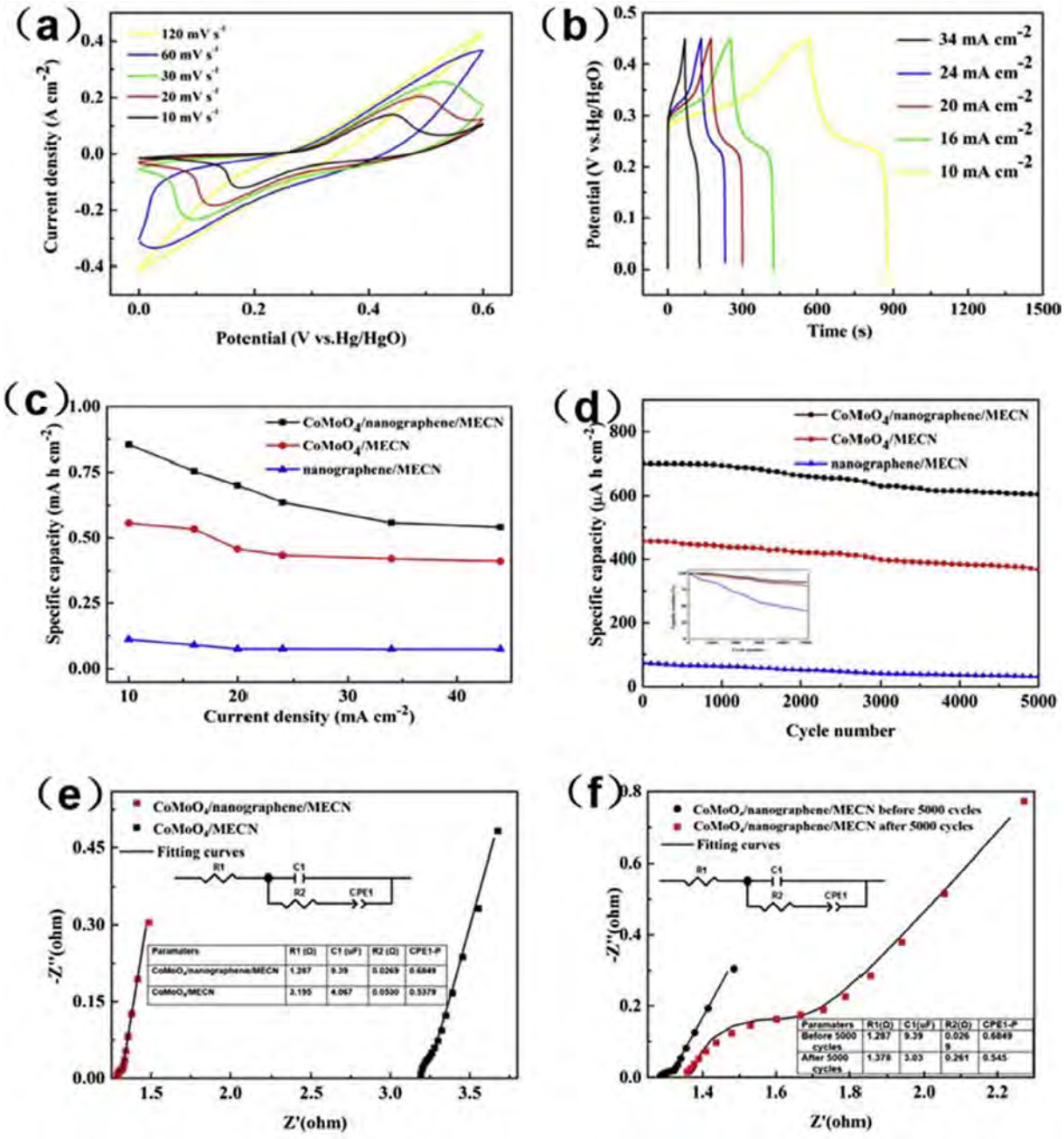

Fig. 8. (a) CV curves of the $CoMoO_4$/nanographene/MECN (2.5 h) electrode at different scanning rates in 2 M KOH; (b) Galvanostatic charging–discharging curves of the $CoMoO_4$/nanographene/MECN (2.5 h) electrode at different current densities; (c) Specific capacity of the nanographene/MECN, $CoMoO_4$/MECN (2.5 h), and $CoMoO_4$/nanographene/MECN (2.5 h) electrodes at various current densities; (d) Cycling stability of the nanographene/MECN, $CoMoO_4$/MECN (2.5 h), and $CoMoO_4$/nanographene/MECN (2.5 h) electrodes at a current density of 20 mA cm^{-2}. with the inset showing the capacity retention of the different electrodes; (e) Nyquist plots of the $CoMoO_4$/nanographene/MECN (2.5 h) and $CoMoO_4$/MECN (2.5 h) electrodes with the inset showing the equivalent circuit and elements fitting the impedance curve; (f) Nyquist plots of the $CoMoO_4$/nanographene/MECN (2.5 h) electrodes before and after 5000 cycles in the long-term performance test with the inset showing the equivalent circuit and elements fitting the impedance curve.

112.4 μW h cm^{-2} and 5.62 mW h cm^{-3} at power densities of 675.5 μW cm^{-2} and 33.78 mW cm^{-3}, respectively, as well as 74.4% capacity retention after 5000 cycles. The nanostructured $CoMoO_4$/nanographene/MECN composite electrode delivers superior electrochemical performance and has large potential in next-generation energy storage devices.

Acknowledgements

This work was jointly supported by Shanghai Pujiang Program (No. 14PJ1403600), National Natural Science Foundation of China (No. 61774060), PCSIRT, Research Innovation Foundation of ECNU (No. 78210245), The Science and Technology Commission of Shanghai Municipality under research grant (No. 14DZ2260800), Scientific Research Foundation for the Returned Overseas Chinese Scholars, State Education Ministry, Open Research Fund of Shanghai Key Laboratory of Multidimensional Information Processing, East China Normal University, as well as City University of Hong Kong Strategic Research Grant (SRG) No. 7004644 and Applied Research Grant (ARG) No. 9667122.

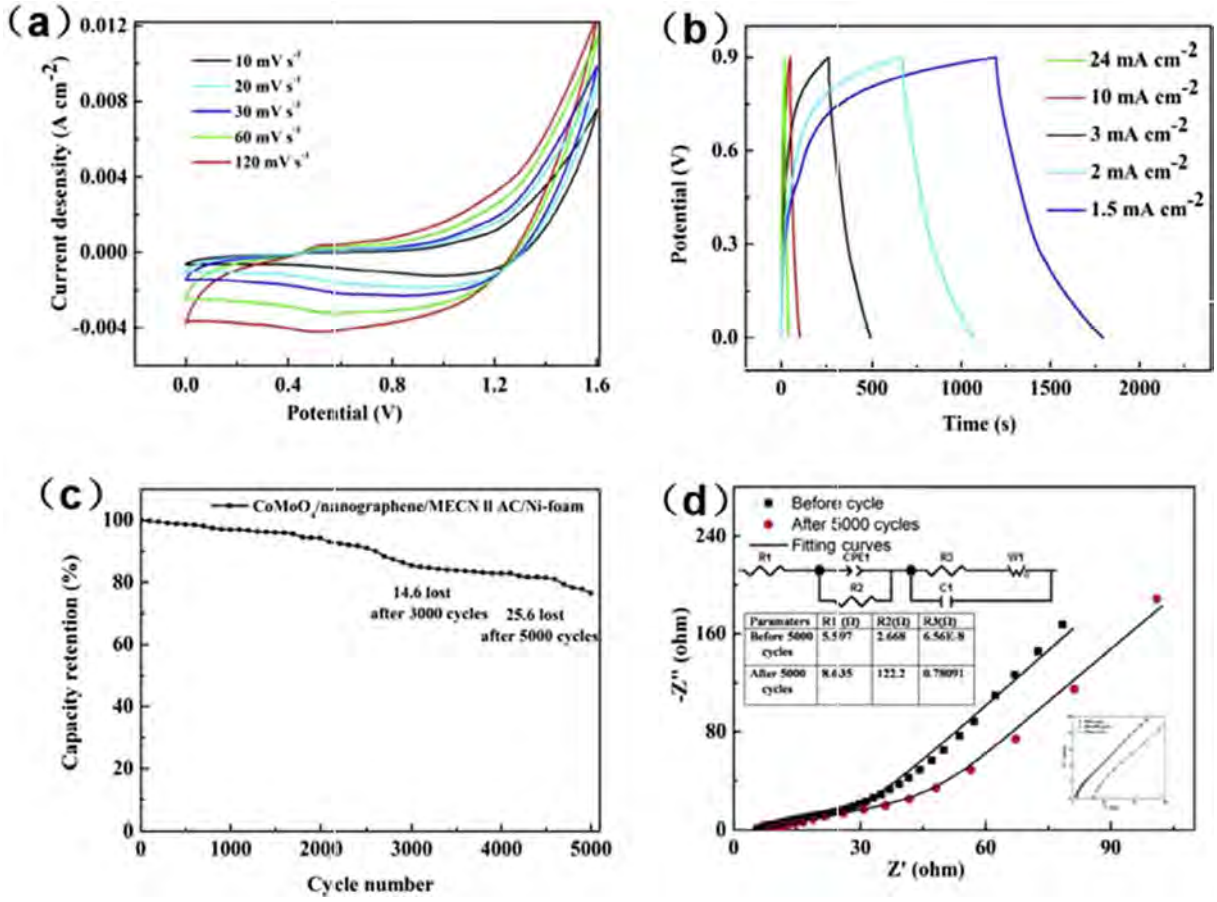

Fig. 9. (a) CV curves of the hybrid device between 0 V and 1.6 V at different scanning rates; (b) Galvanostatic charging–discharging curves of the hybrid device between 0 V and 0.9 V at different current densities; (c) Cycling stability of the hybrid device at a current density of 10 mA cm^{-2}; (d) Nyquist plots of the hybrid device before and after 5000 cycles in the long-term performance test. The inset is the equivalent circuit and elements fitting the impedance curve and magnified high frequency.

References

[1] P. Dhanya, V. Aravindan, M. Srinivasan, S. Ogale, Energy Environ. Sci. 7 (2014) 728–735.
[2] Q. Cheng, J. Tang, J. Ma, H. Zhang, N. Shinya, L.C. Qin, Phys. Chem. Chem. Phys. 13 (2011) 17615.
[3] Y. Wang, G. Cao, Adv. Mater. 20 (2008) 2251–2269.
[4] J.R. Miller, P. Simon, Science 321 (2008) 651–652.
[5] M.F. Warsi, I. Shakir, M. Shahid, M. Sarfraz, M. Nadeem, Z.A. Gilani, Electrochim. Acta 135 (2014) 513–518.
[6] X. Yang, C. Cheng, Y. Wang, L. Qiu, D. Li, Science 341 (2013) 534.
[7] M. Li, C. Liu, H. Cao, H. Zhao, Y. Zhang, Z. Fan, J. Mater. Chem. A 2 (2014) 14844–14851.
[8] H. Kim, M.E. Fortunato, H. Xu, J.H. Bang, K.S. Suslick, J. Phys. Chem. C 115 (2011) 20481–20486.
[9] P. Simon, Y. Gogotsi, B. Dunn, Science 343 (2014) 1210–1211.
[10] T. Brousse, D. Belanger, J.W. Long, J. Electrochem. Soc. 162 (2015) A5185–A5189.
[11] Z. Fan, J. Yan, T. Wei, L. Zhi, G. Ning, T. Li, F. Wei, Adv. Funct. Mater. 21 (2011) 2366–2375.
[12] D. Wu, S. Xu, C. Zhang, Y. Zhu, D. Xiong, R. Huang, R. Qi, L. Wang, P.K. Chu, J. Mater. Chem. A (2016) 4.
[13] Y. Sun, Z. Fang, C. Wang, A. Zhou, H. Duan, Nanotechnology 26 (2015) 374002.
[14] C.W. Kung, H.W. Chen, C.Y. Lin, R. Vittal, K.C. Ho, J. Power Sources 214 (2012) 91–99.
[15] C.C. Hu, K.H. Chang, M.C. Lin, Y.T. Wu, Nano Lett. 6 (2006) 2690.
[16] M. Yang, J.X. Li, H.H. Li, L.W. Su, J.P. Wei, Z. Zhou, Phys. Chem. Chem. Phys. 14 (2012) 11048.
[17] S. Vijayakumar, S. Nagamuthu, G. Muralidharan, Acs Appl. Mater. Interfaces 5 (2013) 2188.
[18] T. Wang, Z. Peng, Y. Wang, J. Tang and G. Zheng, 2013, 3, 2693.
[19] Y. Huang, Y. Huang, W. Meng, M. Zhu, H. Xue, C.S. Lee, C. Zhi, Acs Appl. Mater. Interfaces 7 (2015) 2569.
[20] L. Chen, C. Yuan, B. Gao, S. Chen, X. Zhang, J. Solid State Electrochem. 13 (2009) 1925–1933.
[21] L.Q. Mai, F. Yang, Y.L. Zhao, X. Xu, L. Xu, Y.Z. Luo, Nat. Commun. 2 (2011) 381.
[22] K. Qiu, Y. Lu, D. Zhang, J. Cheng, H. Yan, J. Xu, X. Liu, J.K. Kim, Y. Luo, Nano Energy 11 (2015) 687–696.
[23] Z. Gao, W. Yang, J. Wang, N. Song, X. Li, Nano Energy 13 (2015) 306–317.
[24] G.K. Veerasubramani, K. Krishnamoorthy, J.K. Sang, J. Power Sources 306 (2016) 378–386.
[25] D. Guo, H. Zhang, X. Yu, M. Zhang, P. Zhang, Q. Li, T. Wang, J. Mater. Chem. A 1 (2013) 7247–7254.
[26] K. Chi, Z. Zhang, Q.Y. Lv, C. Xie, J. Xiao, F. Xiao, S. Wang, Acs Appl. Mater. Interfaces 9 (2017) 6044.
[27] M. Li, S. Xu, C. Cherry, Y. Zhu, D. Wu, C. Zhang, X. Zhang, R. Huang, R. Qi, L. Wang, J. Mater. Chem. A 3 (2015) 13776–13785.
[28] M.C. Liu, L.B. Kong, C. Lu, X.M. Li, Y.C. Luo, L. Kang, Mater. Lett. 94 (2013) 197–200.
[29] J. Candler, T. Elmore, B.K. Gupta, L. Dong, S. Palchoudhury, R.K. Gupta, New J. Chem. 39 (2015) 6108–6116.
[30] Z. Xu, Z. Li, X. Tan, C.M.B. Holt, L. Zhang, B.S. Amirkhiz, D. Mitlin, Rsc Adv. 2 (2012) 2753–2755.
[31] X. Xia, L. Wu, Q. Hao, W. Wang, X. Wang, Electrochim. Acta 99 (2013) 253–261.
[32] R. Tan, D. Wu, S. Xu, Y. Zhu, D. Xiong, L. Wang, P. Yang, P.K. Chu, Electrochim. Acta 215 (2016) 515–524.
[33] X. Chen, J. Lin, D. Yuan, P. Ci, P. Xin, S. Xu, L. Wang, J. Micromech. Microeng. 18 (2008) 037003.
[34] Ding Yuan, Pengliang Ci, Fei Tian, Jing Shi, Xu. Shaohui, Peisheng Xin, Lianwei Wang, Large size p-type silicon microchannel plates prepared by photo-electrochemical etching, J. Micro/Nanolith. MEMS MOEMS 8 (2009) 033012.
[35] S. Xu, M. Li, Y. Zhu, L. Wang, P. Yang, P.K. Chu, Electrochim. Acta 132 (2014) 165–171.
[36] C. Liang, D.J. Wu, L.W. Wang, Macro-porous Electrically Conductive Network Process Based on the MEMS Technology (in Chinese), Micronanoelectron. Technol. 53 (5) (2016) 316.
[37] D. Wu, C. Zhang, C. Liang, Y. Zhu, S. Xu, D. Xiong, S. Xue, L. Wang, P.K. Chu, J. Mater. Chem. C 4 (2016) 2079–2087.

[38] D. Wu, S. Xu, M. Li, C. Zhang, Y. Zhu, Y. Xu, W. Zhang, R. Huang, R. Qi, L. Wang, J. Mater. Chem. A 3 (2015) 16695–16707.
[39] J.E.H. And, D.E. Resasco, J. Phys. Chem. B 107 (2003) 3738–3746.
[40] S. Chen, J. Zhu, X. Wu, Q. Han, X. Wang, Acs Nano 4 (2010) 2822.
[41] D. Cai, B. Liu, D. Wang, L. Wang, Y. Liu, H. Li, Y. Wang, Q. Li, T. Wang, J. Mater. Chem. A 2 (2014) 4954–4960.
[42] N. Padmanathan, K.M. Razeeb, S. Selladurai, Ionics 20 (2014) 1323–1334.
[43] Z. Zhang, H. Zhang, X. Zhang, D. Yu, Y. Ji, Q. Sun, Y. Wang, X. Liu, J. Mater. Chem. A (2016) 4.
[44] Z. Gao, F. Wang, J. Chang, D. Wu, X. Wang, X. Wang, F. Xu, S. Gao, K. Jiang, Electrochim. Acta 133 (2014) 325–334.
[45] M. Li, S. Xu, C. Cherry, Y. Zhu, R. Huang, R. Qi, P. Yang, L. Wang, P.K. Chu, Electrochim. Acta 149 (2014) 18–27.